npj | Flexible Electronics

www.nature.com/npjflexelectron

ARTICLE OPEN

Curvy surface conformal ultra-thin transfer printed Si optoelectronic penetrating microprobe arrays

Kyoseung Sim[1], Zhoulyu Rao[1], Yanbin Li[2], Dong Yang[2] and Cunjiang Yu[1,2,3,4]

Penetrating neural probe arrays are powerful bio-integrated devices for studying basic neuroscience and applied neurophysiology, underlying neurological disorders, and understanding and regulating animal and human behavior. This paper presents a penetrating microprobe array constructed in thin and flexible fashion, which can be seamlessly integrated with the soft curvy substances. The function of the microprobes is enabled by transfer printed ultra-thin Si optoelectronics. As a proof-of-concept device, microprobe array with Si photodetector arrays are demonstrated and their capability of mapping the photo intensity in space are illustrated. The design strategies of utilizing thin polyimide based microprobes and supporting substrate, and employing the heterogeneously integrated thin optoelectronics are keys to accomplish such a device. The experimental and theoretical investigations illustrate the materials, manufacturing, mechanical and optoelectronic aspects of the device. While this paper primarily focuses on the device platform development, the associated materials, manufacturing technologies, and device design strategy are applicable to more complex and multi-functionalities in penetrating probe array-based neural interfaces and can also find potential utilities in a wide range of bio-integrated systems.

npj Flexible Electronics (2018)2:2 ; doi:10.1038/s41528-017-0015-8

INTRODUCTION

Electronic devices and systems that can be integrated with the body and thus provide diagnostic and therapeutic functions play vital roles in basic medical research and clinical medicine. The increasing interest in investigating basic neuroscience and applied neurophysiology,[1,2] underlying neurological disorders,[3–6] and understanding and regulating the motor cortex[7,8] has motivated the development of neural interface devices.[9,10] Among various devices, a neural probe array[11–15] that can inject into the brain tissue, record neural activity, and stimulate neurons, represents one of the most important biologically integrated devices and has been successfully developed and extensively used. Owing to its mechanical and electrical properties as well as the well-established manufacturing technologies, bulk silicon based probes have been extensively employed.[12,13,16] To accomplish the probe array, one typical approach involves first defining the electrical paths of the probes on a Silicon (Si) wafer and then isolating them into individual probes in plane, and finally, assembling them into a three-dimensional (3D) array with a rigid support.[13–15,17] The other approach is primarily based on micromachining the Si probes along the thickness direction of a Si wafer to form vertical arrays.[11,12] Both types of probe arrays have been utilized to demonstrate their abilities in neural recording. However, these probes are all relatively rigid and attached to rigid substrates. Issues, including mechanical mismatch between the rigid probe and soft tissue, imperfect contact and poor conformality with the curved surfaces of brain tissues, would lead to tissue damage during motion, especially for chronic implants and for moving animals or humans.[18–20] To eliminate these issues, a few literature have reported flexible probes[21–23] based on biocompatible polymer substrates such as Parylene-C, Polyimide (PI), etc. However, the arrays of the probes are mostly supported by rigid supports that interface with external signal extraction and processing units.[16,24,25] Recently, a flexible probe array was realized through fabricating metal electrodes on a relatively thick flexible polyimide substrate on a handling Si wafer, folding the probes from in-plane to out-of-plane to form an array, and removing the Si wafer by selective dry etching.[22] Such a device involved costly fabrication yet had limited functionality, i.e. mostly electrical potential recording. To solve the challenges in mechanical mismatch from relatively rigid probes, poor conformality to soft and curved surfaces from rigid array support, and to enrich multi-parametric sensing and stimulating functionalities from passive electrodes, a novel device scheme from a full set of device design and fabrication technologies is therefore proposed.

Here we present a 3D penetrating microprobe array in a thin and flexible format, which can attach and conform to curved surfaces and whose function is enabled by transfer printed ultra-thin Si optoelectronics. The thin penetrating microprobes are supported by an ultra-thin PI substrate which renders the ability of conformal attachment to the curved brain. As a proof-of-concept device, a microprobe array with Si photodetector arrays distributed spatially is demonstrated and its capability of mapping the photo intensity in space is illustrated. While the content of this paper primarily focuses on the platform development, the associated materials, manufacturing technologies and device design strategy are applicable to more complex and multi-functionalities in penetrating probe arrays for future advanced neural interfaces, such as high density probes for optogenetic applications.

[1]Materials Science and Engineering Program, University of Houston, Houston, TX 77204, USA; [2]Department of Mechanical Engineering, University of Houston, Houston, TX 77204, USA; [3]Department of Electrical and Computer Engineering, University of Houston, Houston, TX 77204, USA and [4]Department of Biomedical Engineering, University of Houston, Houston, TX 77204, USA
Correspondence: Cunjiang Yu (cyu15@uh.edu)

Received: 29 June 2017 Revised: 7 September 2017 Accepted: 12 October 2017
Published online: 18 January 2018

Published in partnership with Nanjing Tech University

npj nature partner journals

RESULTS

Figure 1a illustrates the schematic architecture of the 3D penetrating microprobe array (4 × 4) with transfer printed ultra-thin Si optoelectronics. The array is supported on a 6 μm thick PI layer with the electrical routines to contact pads that can be bonded with an anisotropic conductive film (ACF) cable to be interfaced with external printed circuit boards for signal extraction. The overlaid structure of each microprobe includes a supporting layer (2 μm) of PI, single crystal Si (1.25 μm) based photodetector, Au electrode (70 nm), PI insulating layer (2 μm), Fe (400 nm), and PI encapsulation layer (2 μm) (inset of Fig. 1a). Each microprobe includes two Si photodetectors, defined by selective doping to enable desired optoelectronic performance based on standard microfabrication processes.[26] The fabricated penetrating microprobe array is shown in Fig. 1b, c. Figure 1d shows an optical microscopic image of a single microprobe. The major fabrication processes of the microprobe array involved transferring ultra-thin Si photodetectors pre-fabricated on a silicon-on-insulator (SOI) wafer, printing them onto thin PI substrate, followed by deposition and patterning of subsequent layers through planar microfabrication, bending the probes vertically through magnetic actuation and finally fixing the probes by epoxy solidification. Figure 2a presents the schematic fabrication process of the microprobe array upon accomplishing the Si photodetector on the SOI wafer. The schematic fabrication processes of the Si photodetector on a SOI wafer are illustrated in Supplementary Fig. 1 and the detailed fabrication processes are described in the Methods section. Figure 2b shows images of the Si photodetector (left) on the SOI wafer, on a polydimethylsiloxane (PDMS) stamp (middle) after retrieving, and on PI substrate (right) after transfer printing. The fabricated photodetector array was transfer printed onto a thin PI layer coated on a temporary supporting glass slide, using a PDMS stamp. Thereafter, Au contact electrodes and interconnects were formed by electron beam evaporation and patterning based on wet chemical etching. An insulating layer of PI was deposited onto the device by spin coating. For magnet actuation, a thin layer of Fe was chosen due to its ferromagnetism with positive and large magnetic susceptibility ($\chi_{m,Fe} = 200{,}000$),[27] which has large permanent magnetizations without an externally applied magnetic field.[28] The Fe layer was formed by electron beam evaporation and lift off process, followed by PI encapsulation. The microprobes were then isolated from the PI substrate by etching through the PI to only leave a hinge near the end using Oxygen plasma dry etching. It is noted that the layers of Si and metals are fully encapsulated. The optical image of a single microprobe after insulation is shown in Fig. 2c. Wet chemical sacrificial releasing of the microprobes from the glass substrate was performed based on buffered oxide etchant (BOE, 6:1) etching. Small droplets of liquid epoxy SU-8 (2010, Microchem) were placed on the hinge of each microprobe by a micro-positioner. Using a bulk neodymium magnet (K&J Magnetics, Inc. N52), an external magnetic field (maximum 0.767 T at edge) was applied to bend the microprobes vertically. The SU-8 drops were solidified by ultraviolet (UV, 365 nm) light and baked to fix the position of the microprobes. Figure 2d presents the completed 3D penetrating microprobe array.

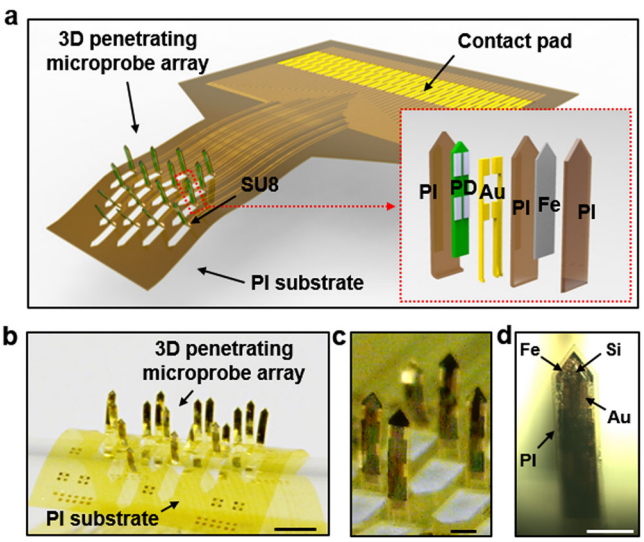

Fig. 1 Flexible 3D penetrating microprobe array. **a** A schematic illustration of the flexible 3D penetrating microprobe array. The inset is an exploded structure of a single probe. **b** An optical image of 3D penetrating microprobe array on a curved surface. (scale bar, 2 mm). **c** An optical image of microprobes. (scale bar, 500 μm). **d** An optical microscopic image of a single microprobe. (scale bar, 500 μm)

Analytical calculations were also performed to verify the actuation experiment. To ensure successful actuation, the torque induced by the magnet needs to overcome the internal torque of the hinge.[29] Since the length of the Fe is much larger than its thickness, the induced torque T_{mag} can be written as

$$T_{mag} = L_{Fe}T_{Fe}W_{Fe}IH_{ext}\cos\theta \quad (1)$$

where L_{Fe}, T_{Fe}, and W_{Fe} are the length, thickness and width of the Fe respectively, I is the magnetization of Fe, H_{ext} is the external magnetic field (as shown in Supplementary Fig. 2), and θ is the bending angle. To let the magnet induced torque equal to the internal torque, one can get

$$L_{Fe}T_{Fe}W_{Fe}IH_{ext}\cos\theta = E_h\frac{W_hT_h^3}{12L_h}\theta \quad (2)$$

where L_h, T_h, W_h, and E_h are the length, thickness, width, and Young's modulus of the PI hinge, respectively. Therefore the relationship between the bending angle and the applied magnetic field can be built into the following equation:

$$f(\theta) = \frac{\theta}{\cos\theta} = 12IH_{ext}\frac{L_hL_{Fe}T_{Fe}W_{Fe}}{E_hW_hT_h^3} \quad (3)$$

The details of the calculations are presented in Supplementary Information. Supplementary Fig. 3 plots the theoretical magnetic field depending on bending angle. Based on the calculations above, magnetic field of 0.644 T is required to achieve a bending angle of 70°. The sequential optical images of the bending microprobe are illustrated in Supplementary Fig 4.

The photodetector employs two n-p Si diodes configured in back to back (n-p-p-n) fashion. Figure 3a shows an optical microscopic image of the Si photodetectors along the probe. The dimensions of Si membrane and doping area are 270 μm × 1.85 mm and 110 μm × 360 μm, respectively. The distance between the two photodetectors is 700 μm. The photocurrent depending on applied bias at different levels of light intensity is shown in Fig. 3b. The photocurrent of the device under illumination at a light intensity of 5430 lx is 5.583×10^{-7} A, and the dark current is 4.907×10^{-10} A at 3 V bias. The calculated current ratio $\Delta I/I_o$, i.e. the ratio between the current change ΔI from dark (I_o) to illumination ($I_{illumination}$) conditions and the dark current, is 1136 at 3 V bias.[30,31] Figure 3c plots the calibration curve including current change as a function of light intensity, in which a typical linear trend was obtained. The dynamic photo response of the device was characterized and shown in Fig. 3d. The current was measured at a bias of 3 V with the light repetitively ON and OFF.

Since the microprobes are so thin and easily deformed (Fig. 3e), the performance of the optoelectronics upon mechanical bending have been investigated to ensure its fidelity of light intensity sensing. The devices were characterized when bent along a longitudinal direction at various bending radii as shown in Fig. 3f. The current under illumination and in dark at a bias of 3 V is

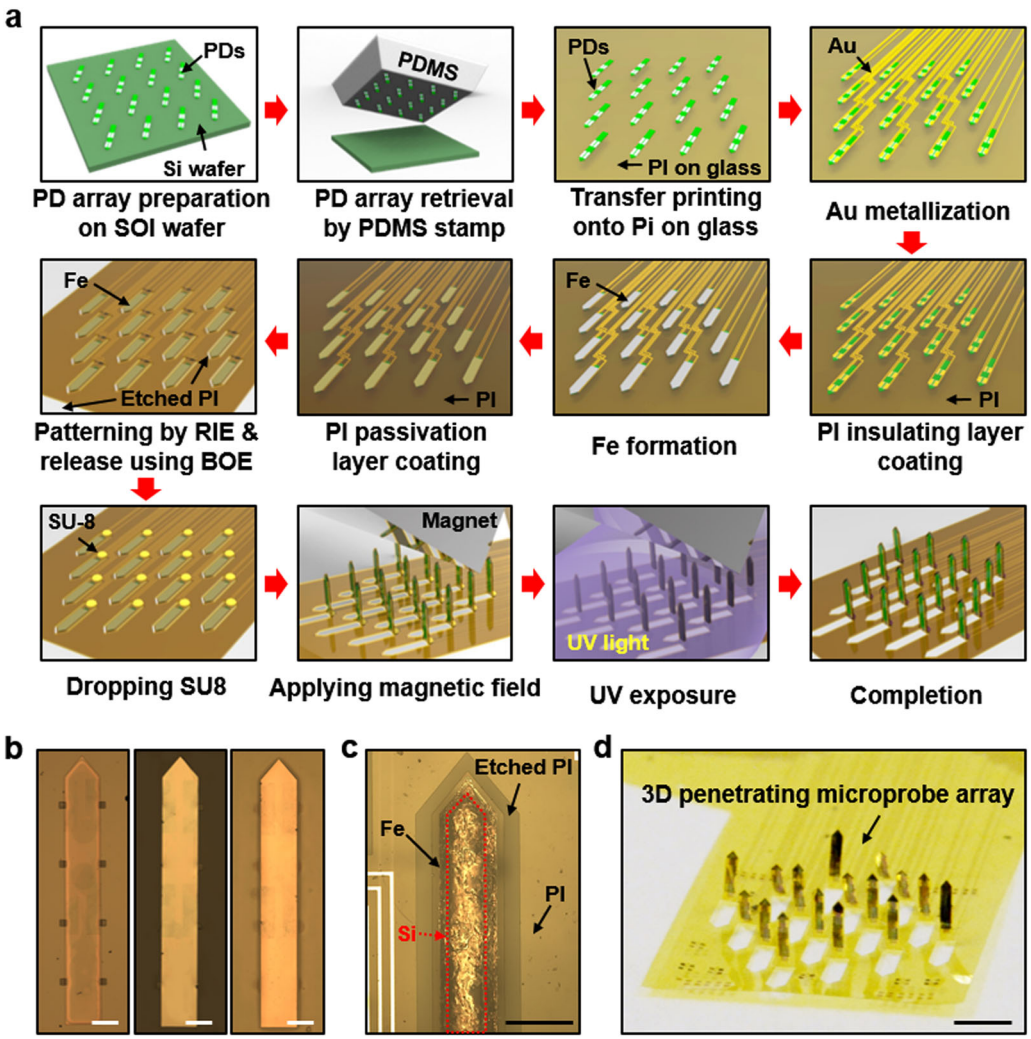

Fig. 2 Fabrication process for the penetrating microprobe array. **a** A schematic illustration for the fabrication of 3D penetrating microprobe array. **b** Optical microscopic images of needle shaped Si with photodetectors (left) on an SOI wafer, (middle) on a PDMS stamp, (right) on a PI after transfer printing. (scale bar, 200 μm). **c** An optical image of completed single microprobe after isolation. (scale bar, 500 μm) **d** An optical image of a fabricated penetrating microprobe array. (scale bar, 2 mm)

shown Fig. 3g. The dark current and photocurrent under illumination have a negligible decrease at relativly large bending radii (e.g. >8 mm), yet decrease up to 7.9% once the bending radius is down to 1.3 mm. Although the photocurrent and dark current slightly decreased as a result of bending, the ratio between them remained invariant, as shown in blue line on Fig. 3g. Analytical studies based on a simplified multilayered beam model were performed to extract the mechanical strain in the Si. A multiple layered composite structure is modeled, as shown in Supplementary Fig. 5. The detailed analysis is described in supporting information. The calculated strain of the Si (along the top, middle, and bottom planes) is plotted in Supplementary Fig. 6. At a bending radius of 1 mm, the strain along the middle plane is about 0.05% and the maximum tensile strain is about 0.11%. The results indicate that no mechanical fracture in the brittle Si would occur since the bending induced strain is far less than the fracture limit (1%) of Si. Together with its mechanical reliability, the stable current ratio under bending conditions suggests that the optoelectronic microprobes is feasible to capture the photo intensity even though they are deformed after future insertion.

Because the holding PI substrate is very thin, the array can be easily bent and forms conformal contact with curvilinear surfaces.[20] Figure 4a, b show images of the 3D penetrating microprobe array on curvilinear concave and convex surfaces, respectively. To illustrate the potential ability of penetrating into brain tissue, the 3D microprobe array was inserted into a human brain model that was made by solidified gelatin mimicking the soft tissue. It is noted that the Si improves the rigidity of the microprobes to faciliate the success of insertion. The stiffness of the microprobes can be tuned by changing the designs, e.g. the thickness of the transfer printed Si, or PI. Supplementary Table 1 shows a comparison of mechanical properties with other reported works depending on structure and materials. Supplementary Fig. 7 shows the sequential optical images of a microprobe that was successfully inserted into a piece of gelatin. As shown in Fig. 4c, the device attaches to the wrinkled surface of the brain model and conforms with the curvatures (radius of $R_{convex} \sim 6.1$ mm and $R_{concave} \sim 1.7$ mm) while the microprobes are inserted within the gelatin brain model. All these experimental verfications suggest that the 3D penetrating microprobe array can form intimate contact and create seamless integration with the soft curvy surfaces, which is a highly favorable feature for neural interface devices.

The feasibility of mapping the light intensity within the soft substances spatially was also verified, which has relevance in

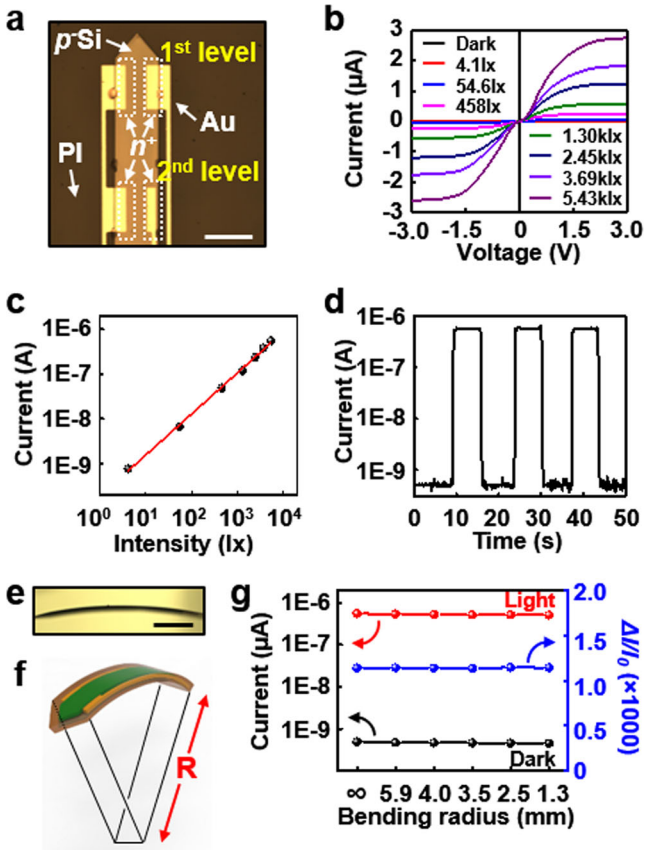

Fig. 3 Characterization of the optoelectronic microprobe. **a** An optical microscopic image of a microprobe with two photodetectors and the metal interconnects. (scale bar, 300 μm) **b** I–V characteristics at different light intensities. **c** Calibration curve of the Si photodetector. **d** Dynamic photo response characteristic at 3 V of constant bias. **e** An optical microscopic side view image of a single probe. (scale bar, 500 μm) **f** Schematic illustration of a bent microprobe. **g** The measured current in dark and under illumination, and calculated $\Delta I/I_0$ at different bending radii

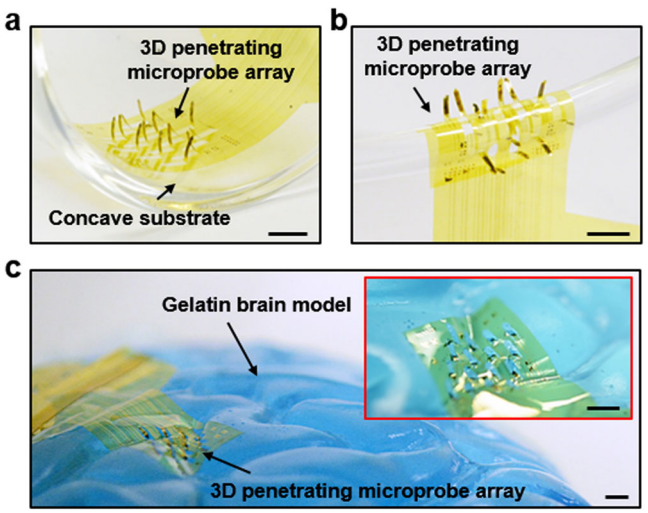

Fig. 4 Deformation of flexible 3D penetrating microprobe array on curvilinear surface. 3D penetrating microprobe array on (**a**) a concave surface, (**b**) a convex surface, and (**c**) a gelatin human brain model. The inset in **c** is an optical image from different angle of view. (scale bar, 3 mm)

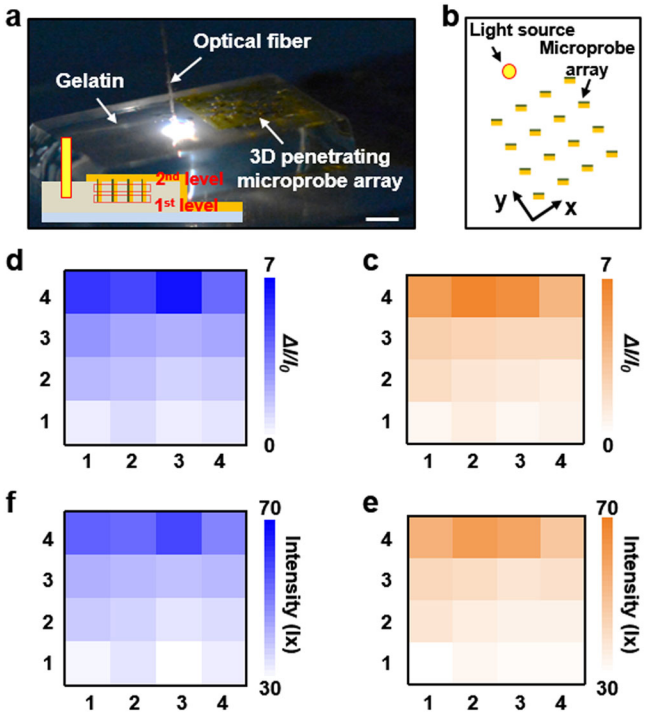

Fig. 5 Demonstration of the light intensity mapping. **a** Optical image of the experimental setup. The inset is the schematic front view of the setup. (scale bar, 5 mm) **b** Schematic top view of the injected light source and microprobe array. **c**, **d** The photocurrent maps from the first level **c** and the second level **d** of photodetectors on the microprobes. **e**, **f** The light intensity maps from the photodetectors at the first level and the second level, respectively

optogenetic applications. Optogenetics involves injecting light into the brain to stimulate or control neurons. Knowing the light intensity in spatial positions can facilitate the understanding of the biological consequences. The microprobe array can serve for this purpose. The light intensity distribution in gelatin was measured by a 3D penetrating microprobe array. The experiment setup is shown in Fig. 5a, where the microprobes were inserted in gelatin with an optical fiber light source injected nearby. The photodetectors on the microprobes can sense the light intensity at a specific spatial location, as illustrated in Fig. 5b. Figure 5c, d shows the normalized photocurrent maps from the 4×4 microprobes near and far from the tips, which is consistent with our expectations. The normalized current responses over time (dark → illumination → dark) for each photodetector are shown in Supplementary Figs. 8 and 9. Based on the measured photocurrent, light intensity can be as shown in Fig. 5e, f. The results indicate that the optoelectronic microprobe array can effectively measure the photocurrent, and thus map light intensity in spatial distribution.

DISCUSSION

In summary, the 3D optoelectronic penetrating microprobes array presented in this study overcomes the existing challenges in mechanical mismatch and features seamless integration with the soft curvy surfaces. Instead of using bulk and rigid Si to provide multi-functionality, the transfer printed ultra-thin Si optoelectronics on the thin microprobes suggests a viable avenue to achieve those capabilities while bypassing the mechanical mismatch issue. The presented photo intensity mapping capability serves as an example of the enabled functionality from the ultra-thin Si electronics. The experimental and theoretical investigations illustrate the key materials, manufacturing, and mechanical

aspects. The design strategies of utilizing thin PI based microprobes and the supporting substrate, and the transfer printed optoelectronics is a key. The magnetic actuation of the probes from a planar to a 3D vertical array proves to be effective in such a thin device. By taking the advantage of the recent advances in heterogeneous integration,[32–36] this type of penetrating microprobe array could be equipped with other functionalities such as sensors, actuators, light sources, not just limited to Si electronics, for penetrating probe array based neural interfaces with more complex and multi-functionalities, and can also find potential and broad utilities in a wide range of bio-integrated applications, such as optogenetics, deep brain stimulation, cortex mapping, etc.

METHODS

Fabrication of Si photodetectors

The Si photodetector is fabricated using an SOI wafer with a 1.25 μm thick top silicon layer, where the procedure have been reported elsewhere.[37] The fabrication of devices began with forming 300 nm thick SiO_2 doping mask prepared by spin-on-glass (700B, Filmtronics) coating, photolithography, and wet etching using BOE (1:6). To implement selective doping, phosphorous based spin-on-dopant (P510, Filmtronics) was used for the doping process at 950 °C to form two back to back n-p-p-n diodes by taking advantage of the slightly doped (resistivity: 11.5 Ω cm) p-type Si. The top Si was patterned into a needle shape array with two photodetectors by reactive ion etching (RIE) based on sulfur hexafluoride (SF_6) gas. After removing the exposed SiO_2 in BOE, photoresist anchors were formed by photolithography to prevent the floating away of thin Si array after fully undercut etching of SiO_2. The photodetector array was then fully immersed in concentrated hydrofluoric acid (HF, 49%) to remove the underneath SiO_2, thus, separating the Si array from the thick Si wafer.

Transfer printing of Si photodetector array onto PI

The array of devices was retrieved by using a 8 mm thick PDMS (Sylargd 184) stamp. Thereafter, polyimide (PI) precursor solution (PI-2545, HD Micro Systems) was coated on a cleaned temporary glass substrate and the Si array on the PDMS stamp was then printed onto the half cured PI, followed by curing at 250 °C for 1 h.

Penetrating microprobe array fabrication

After transfer printing the Si array onto the PI, Au interconnects were formed by electron beam evaporation and patterning using conventional photolithography and a wet etching process using gold etchant (Type TFA, Transene Co. Inc). Thereafter, a thin insulating PI was spin coated on top of the devices and cured at 250 °C for 1 h. Then a 400 nm thick Fe layer was deposited by electron beam evaporation and patterned based on a lift-off process. A third layer of PI as encapsulation was spin coated and cured, followed by patterning by reactive ion etching (RIE, O_2, 40 sccm, 150 mTorr, 250 W, 25 min) with a SiO_2 mask. The thin device was then separated from the glass substrate using buffer oxide etchant (BOE, 6:1). Small droplets of epoxy SU-8 (SU-8 2010, MicroChem) were placed on the designed hinges and baked at 95 °C to remove the solvent. To actuate the microprobes microneedle, a neodymium magnet (K&J Magnetics, Inc. N52, 50.6 mm × 50.6 mm × 12.5 mm) was applied to the needles. The vertically standing array was accomplished by solidifying the SU-8 under ultraviolet light exposure (UV75 Light, THORLABS) while under magnetic actuation. The structural configurations of the 3D microprobe array was fixed even after removing the magnet.

Gelatin human brain model preparation

The gelatin brain model was prepared by mixing and dissolving gelatin powder (3.5 wt%, Knox®) within blue-dyed DI water at 90 °C, followed by replica molding of an Ecoflex based human brain model after solidifying the solution.

Device characterization

The electrical characteristics of fabricated Si photodetectors were characterized using a Keithley 4200-SCS parameter analyzer. The injected light was based on a 0.2 mm diameter optical fiber (ThorLabs) that is equipped with a visible light source (LS-1, Ocean Optics).

Data availability

The authors declare that the main data supporting the findings of this study are available within the paper and its Supplementary Information document. Other relevant data are available from the corresponding author upon request.

ACKNOWLEDGEMENTS

This work is partially supported by NSF grants (1509763, 1554499), the Startup Fund and Bill D. Cook Faculty Scholarship from the University of Houston.

AUTHOR CONTRIBUTIONS

K.S., and C.Y. conceived the idea of this research. K.S., Z.R. and C.Y. designed the experiment. Y.L. performed numerical analysis. K.S., Z.R., D.Y. and C.Y. performed the experiment and analysis. K.S. and C.Y. co-wrote the paper.

ADDITIONAL INFORMATION

Supplementary information accompanies the paper on the *npj Flexible Electronics* website (https://doi.org/10.1038/s41528-017-0015-8).

Competing interests: The authors declare that they have no competing financial interests.

Publisher's note: Springer Nature remains neutral with regard to jurisdictional claims in published maps and institutional affiliations.

REFERENCES

1. Brock, C. et al. Neurophysiology and new techniques to assess esophageal sensory function: an update. *Ann. N.Y. Acad. Sci.* **1380**, 78–90 (2016).
2. Rodriguez, J. et al. Increased densities of resting and activated microglia in the dentate gyrus follow senile plaque formation in the CA1 subfield of the hippocampus in the triple transgenic model of Alzheimer's disease. *Neurosci. Lett.* **552**, 129–134 (2013).
3. Freund, P. et al. Embodied neurology: an integrative framework for neurological disorders. *Brain* **139**, 1855–1861 (2016).
4. Small, S. A. & Petsko, G. A. Retromer in Alzheimer disease, Parkinson disease and other neurological disorders. *Nat. Rev. Neurosci.* **16**, 126–132 (2015).
5. Stam, C. J. Modern network science of neurological disorders. *Nat. Rev. Neurosci.* **15**, 683–695 (2014).
6. Chang, E. F. Towards large-scale, human-based, mesoscopic neurotechnologies. *Neuron* **86**, 68–78 (2015).
7. McBride, S. D., Parker, M. O., Roberts, K. & Hemmings, A. Applied neurophysiology of the horse; implications for training, husbandry and welfare. *Appl. Anim. Behav. Sci.* **190**, 90–101 (2017).
8. Stoesz, B. M., Hare, J. F. & Snow, W. M. Neurophysiological mechanisms underlying affiliative social behavior: insights from comparative research. *Neurosci. Biobehav. Rev.* **37**, 123–132 (2013).
9. Shen, W. et al. Extracellular matrix-based intracortical microelectrodes: toward a microfabricated neural interface based on natural materials. *Microsyst. Nanoeng.* **1**, 15010 (2015).
10. Borton, D. A., Yin, M., Aceros, J. & Nurmikko, A. An implantable wireless neural interface for recording cortical circuit dynamics in moving primates. *J. Neural. Eng.* **10**, 026010 (2013).
11. Jones, K. E., Campbell, P. K. & Normann, R. A. A glass/silicon composite intracortical electrode array. *Ann. Biomed. Eng.* **20**, 423–437 (1992).
12. Nordhausen, C. T., Rousche, P. J. & Normann, R. A. Chronic recordings of visually evoked responses using the utah intracortical electrode array. In: Szeto, A. Y. J. & Rangayyan, R. M. (eds) Paper presented at the *Conf. Proc. IEEE Eng. Med. Biol. Soc*. 1391–1392 (IEEE, San Diego, CA, USA, 1993).
13. Hoogerwerf, A. C. & Wise, K. D. A three-dimensional microelectrode array for chronic neural recording. *IEEE Trans. Biomed. Eng.* **41**, 1136–1146 (1994).
14. Kim, C. & Wise, K. D. A 64-site multishank CMOS low-profile neural stimulating probe. *IEEE J. Solid-State Circuits* **31**, 1230–1238 (1996).
15. Bai, Q., Wise, K. D. & Anderson, D. J. A high-yield microassembly structure for three-dimensional microelectrode arrays. *IEEE Trans. Biomed. Eng.* **47**, 281–289 (2000).
16. Norlin, P., Kindlundh, M., Mouroux, A., Yoshida, K. & Hofmann, U. G. A 32-site neural recording probe fabricated by DRIE of SOI substrates. *J. Micromech. Microeng.* **12**, 414 (2002).
17. Musallam, S., Bak, M. J., Troyk, P. R. & Andersen, R. A. A floating metal microelectrode array for chronic implantation. *J. Neurosci. Methods.* **160**, 122–127 (2007).

18. Byun, D., Cho, S. J. & Kim, S. Fabrication of a flexible penetrating microelectrode array for use on curved surfaces of neural tissues. *J. Micromech. Microeng.* **23**, 125010 (2013).
19. Xiang, Z., Liu, J. & Lee, C. A flexible three-dimensional electrode mesh: An enabling technology for wireless brain–computer interface prostheses. *Microsyst. Nanoeng.* **2**, 16012 (2016).
20. Kim, D.-H. et al. Dissolvable films of silk fibroin for ultrathin conformal bio-integrated electronics. *Nat. Mater.* **9**, 511–517 (2010).
21. Lee, K.-K. et al. Polyimide-based intracortical neural implant with improved structural stiffness. *J. Micromech. Microeng.* **14**, 32 (2003).
22. Takeuchi, S., Suzuki, T., Mabuchi, K. & Fujita, H. 3D flexible multichannel neural probe array. *J. Micromech. Microeng.* **14**, 104 (2004).
23. Kim, T.-i et al. Injectable, cellular-scale optoelectronics with applications for wireless optogenetics. *Science* **340**, 211–216 (2013).
24. John, J., Li, Y., Zhang, J., Loeb, J. A. & Xu, Y. Microfabrication of 3D neural probes with combined electrical and chemical interfaces. *J. Micromech. Microeng.* **21**, 105011 (2011).
25. Wang, M.-F., Maleki, T. & Ziaie, B. A self-assembled 3D microelectrode array. *J. Micromech. Microeng.* **20**, 035013 (2010).
26. Huang, X. et al. Biodegradable materials for multilayer transient printed circuit boards. *Adv. Mater.* **26**, 7371–7377 (2014).
27. Schenck, J. F. The role of magnetic susceptibility in magnetic resonance imaging: MRI magnetic compatibility of the first and second kinds. *Med. Phys.* **23**, 815–850 (1996).
28. Kasap, S. O. *Principles of Electronic Materials and Devices*, 3rd edn. 699 (McGraw-Hill Higher Education, New York, NY, 2006).
29. Iwase, E., Takeuchi, S. & Shimoyama, I. Sequential batch assembly of 3-D microstructures with elastic hinges by a magnetic field. In: Gianchandani, Y. B. & Tai, Y. C. (eds) Paper presented at the *MEMS 2002 International Conference*, 188–191 (IEEE, Las Vegas, NV, USA, 2002).
30. Noh, Y.-Y., Kim, D.-Y. & Yase, K. Highly sensitive thin-film organic phototransistors: effect of wavelength of light source on device performance. *J. Appl. Phys.* **98**, 074505 (2005).
31. Liu, X. et al. All-printable band-edge modulated ZnO nanowire photodetectors with ultra-high detectivity. *Nat. Commun.* **5**, 4007 (2014).
32. Meitl, M. A. et al. Transfer printing by kinetic control of adhesion to an elastomeric stamp. *Nat. Mater.* **5**, 33–38 (2006).
33. Feng, X. et al. Competing fracture in kinetically controlled transfer printing. *Langmuir.* **23**, 12555–12560 (2007).
34. Yoon, J. et al. Ultrathin silicon solar microcells for semitransparent, mechanically flexible and microconcentrator module designs. *Nat. Mater.* **7**, 907–915 (2008).
35. Carlson, A., Bowen, A. M., Huang, Y., Nuzzo, R. G. & Rogers, J. A. Transfer printing techniques for materials assembly and micro/nanodevice fabrication. *Adv. Mater.* **24**, 5284–5318 (2012).
36. Yu, C. et al. Adaptive optoelectronic camouflage systems with designs inspired by cephalopod skins. *Proc. Natl. Acad. Sci. U.S.A.* **111**, 12998–13003 (2014).
37. Sim, K. et al. High fidelity tape transfer printing based on chemically induced adhesive strength modulation. *Sci. Rep.* **5**, 16133 (2015).